Earth, Planets and Space

FULL PAPER Open Access

Dual-frequency to five-frequency real-time precise point positioning using new BDS-3 PPP-B2b service

Haochen Yang[1], Xiaodong Ren[1,2*], Mingxiu Liu[1] and Xiaohong Zhang[1,2,3]

Abstract

BeiDou global navigation satellite system (BDS-3), a developed GNSS by China, has the ability to support five different signals, including B1I, B3I, B1C, B2a, and B2b. Meanwhile, BDS-3 has officially provided the satellite-based precise point positioning (PPP) service through the B2b signal (PPP-B2b) since 2021. It's necessary to conduct a comprehensive analysis on multi-frequency PPP with PPP-B2b corrections. In this study, a multi-frequency undifferenced and uncombined PPP model (UDUC) using PPP-B2b corrections was employed to investigate dual-frequency to five-frequency real-time PPP performance. The results show that compared with the conventional dual-frequency solutions, multi-frequency solutions can improve both the convergence performances and positioning accuracy of PPP-B2b service, especially during the convergence stage. The quad-frequency and five-frequency solutions can achieve the best positioning performance. The static solutions of multi-frequency PPP models reach the centimeter-level accuracy after convergence. In kinematic mode, the convergence time of the five-frequency PPP results is reduced by 23.5% compared with the dual-frequency results. The root mean square (RMS) errors of the five-frequency PPP in the E, N, and U components are 7.1 cm, 4.8 cm, and 12.4 cm, which are improved by 6.8%, 11.5%, and 5.5%, respectively.

Keywords Precise point positioning (PPP), Multi-frequency, PPP-B2b, BDS-3, GNSS

*Correspondence:
Xiaodong Ren
xdren@whu.edu.cn
Full list of author information is available at the end of the article

Graphical Abstract

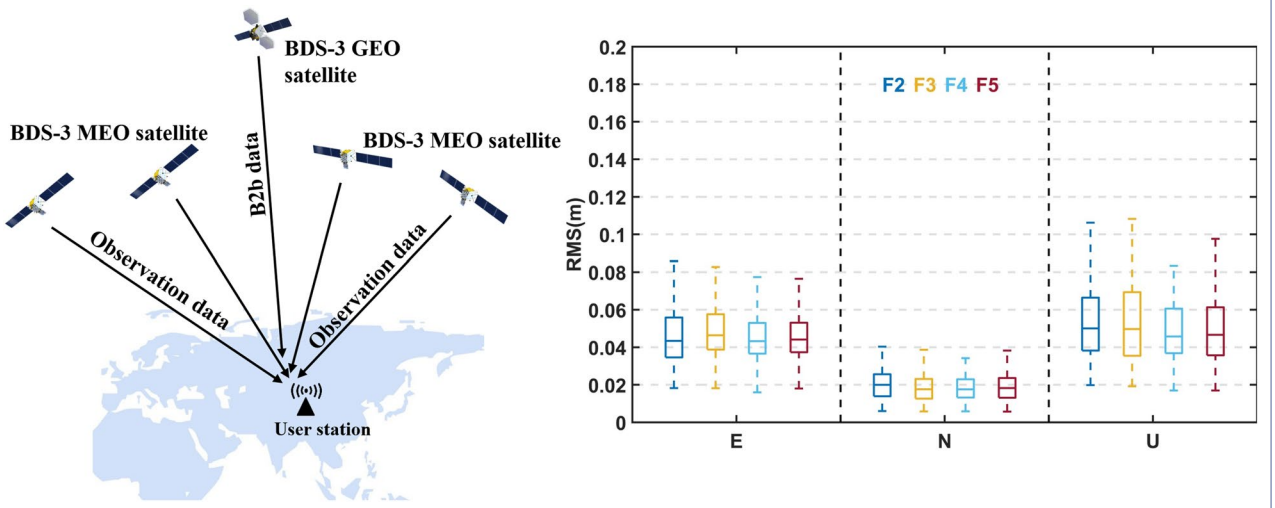

Introduction

Precise point positioning (PPP) technology is considered an important method to obtain centimeter-level positioning accuracy using a single receiver in any location worldwide (Zumberge et al. 1997, Kouba and Héroux 2001). In order to meet the increasing demand of real-time PPP, the International GNSS Service (IGS) launched Real-Time Pilot Project in 2007, and officially released Real-Time Service (RTS) in 2013 (Elsobeiey and Al-Harbi 2016; Kazmierski et al. 2020). The users with real-time needs can obtain highly accurate real-time satellite orbit and clock products via the Internet. Unfortunately, the instability of Internet can make RTS unavailable. Some commercial companies have started to generate real-time products based on their own global GNSS station networks and broadcast them through satellite links (Booth and Snow 2009, Leandro et al. 2011). For example, StarFire SF3 provides real-time users with GPS and GLONASS orbits, clock offsets, uncalibrated phase delay products based on about 60 GNSS stations worldwide (Dai et al. 2016).

Currently, BDS-3, Galileo, and QZSS all provide real-time PPP service for free (CSNO 2020b; Zhang et al. 2020, 2022; Chen et al. 2022; Ilaria et al. 2023; Namie et al. 2018). Compared with RTS, these satellite-based services use navigation signal to transmit real-time products without other auxiliary means. Thus, they're able to provide reliable, continuous service in the event of Internet outages or instability. The Galileo High Accuracy Service (HAS) uses E6B signal to transmit satellite orbits, clock offsets, code bias, phase bias and atmospheric delay corrections (Rovira-Garcia et al. 2021; Naciri et al. 2023). The HAS aims to achieve 20 cm in the horizontal direction, and 40 cm in the vertical direction within 300 s in the European region (Fernandez-Hernandez et al. 2022). The QZSS L6D signal provides Centimeter Level Augmentation Service (CLAS) over Japan and the surrounding area. The CLAS can achieve centimeter-level positioning accuracy within 1 min (Hao et al. 2020). The PPP service provided by BDS-3 uses B2b signals from three geosynchronous orbit satellites (GEO) to broadcast real-time corrections for GPS and BDS-3 satellites (Yang et al. 2019).

Research by scholars and institutions has been carried out to evaluate PPP-B2b service. Song et al. (2021), Huang and Meng (2021) comprehensively evaluated the quality of PPP-B2b corrections based on international GNSS Monitoring and Assessment System station data in China. The positioning accuracy achieved centimeter-level for static solutions and decimeter-level for kinematic solutions. Xu et al. (2021) pointed out that the PPP-B2b corrections can effectively correct the discontinuous error caused by broadcast ephemeris update. Tao et al. (2021) compared the PPP-B2b corrections with the CNES real-time corrections and discussed the matching characteristics of the corrections. This work pointed out that due to the worse GPS signal-in-space range error (SISRE) compared with BDS SISRE, the average convergence time of the GPS-only solution was 64.4 min, which was significantly longer than that of the BDS-only solution. Sun et al. (2023) analyzed the long-term performance based on PPP-B2b corrections of nearly 1 year. This work found that a constant bias

in clock offset causes much longer convergence time. Yang et al. (2022) sorted out the differences between PPP-B2b and BDS satellite-based augmentation service. The research by Zhou et al. (2023) showed that by applying the PPP-B2b corrections, the accuracy of the single-frequency PPP is better than 0.3 m in the horizontal direction and 0.6 m in the vertical direction, respectively. Xu et al. (2023) estimated signal in space range errors to reduce the effects of remaining PPP-B2b orbit errors and clock errors and improved positioning performance. Wu et al. (2023) and Geng et al. (2022) confirmed the potential of PPP-B2b service in various real-time user situations, especially at highly kinematic platforms and ocean environments. Their work expands the boundaries of PPP-B2b applications. Some other researchers have also conducted preliminary experiments based on PPP-B2b corrections to verify the service performance (Ren et al. 2021; Tang et al. 2022; Liu et al. 2022; Zhou et al. 2022; He et al. 2023).

In addition to the conventional B1I and B3I signals, BDS-3 has the ability to support three new signals with advanced signal structure and better strength, which are B1C, B2a and B2b (Jin and Su 2020; Li et al. 2020; Wu et al. 2022). Current research on PPP-B2b mostly focuses on legacy dual-frequency solution and doesn't make full use of BDS-3 new signals. The potential for better positioning performance with multi-frequency GNSS observations and PPP-B2b corrections is worth investigating. First, we introduced the method to obtain precise real-time orbits and clock offsets from PPP-B2b corrections and evaluated the quality of PPP-B2b real-time corrections. Then, a multi-frequency PPP model using BDS-3 PPP-B2b service was employed. Finally, the static and kinematic dual-frequency to five-frequency PPP performance using data from several IGS stations were analyzed in detail.

Methodology

Processing method of PPP-B2b corrections

Several types of corrections are provided in PPP-B2b service through B2b signal, including precise satellite orbits, clock offsets, and difference code bias (DCB). The update intervals of satellite orbit, clock offsets, and DCB correction are 48 s, 6 s and 48 s, respectively. The valid time of satellite orbit correction is 96 s while that of satellite clock offset correction is 12 s. Due to the stability of satellite DCB, the valid time of DCB provided by PPP-B2b is 86,400 s. The current service area is 80°E–155°E, 5°S–55°N. The BeiDou Navigation Satellite System Time and the BeiDou Coordinate System are used for the time reference and the coordinate system, respectively (CSNO 2020a). As of March 2023, PPP-B2b service can support 27 BDS-3 satellites from C19 to C46 (except for C31) and GPS satellites in China and the surrounding area (Tao et al. 2021). Issues of Data (IOD) are defined to identify the corrections. If the IOD of navigation (IODN) of the orbit correction matches with the IOD of the clock (IODC) from the broadcast ephemeris, the precise satellite orbits can be obtained using Eq. (1) and Eq. (2):

$$\boldsymbol{X}_{B2b} = \boldsymbol{X}_{brdc} - \Delta\boldsymbol{X}, \tag{1}$$

where $\boldsymbol{X}_{B2b}$ is the corrected real-time satellite orbit. $\boldsymbol{X}_{brdc}$ presents the satellite orbit generated from the broadcast ephemeris. $\Delta\boldsymbol{X}$ is the PPP-B2b orbit correction in the Earth-Centered-Earth-Fixed (ECEF) frame, which can be calculated as follows:

$$\begin{cases} \boldsymbol{e}_{\boldsymbol{R}} = \dfrac{\boldsymbol{r}}{|\boldsymbol{r}|} \\ \boldsymbol{e}_{\boldsymbol{C}} = \dfrac{\boldsymbol{r} \times \dot{\boldsymbol{r}}}{|\boldsymbol{r} \times \dot{\boldsymbol{r}}|} \\ \boldsymbol{e}_{\boldsymbol{A}} = \boldsymbol{e}_{\boldsymbol{C}} \times \boldsymbol{e}_{\boldsymbol{R}} \\ \Delta\boldsymbol{X} = \left[\boldsymbol{e}_{\boldsymbol{R}} \ \boldsymbol{e}_{\boldsymbol{A}} \ \boldsymbol{e}_{\boldsymbol{C}} \right] \Delta\boldsymbol{O} \end{cases}, \tag{2}$$

where $\boldsymbol{r}$ and $\dot{\boldsymbol{r}}$ are the satellite position and velocity vectors generated from the broadcast ephemeris, respectively. $\Delta\boldsymbol{O}$ represents the PPP-B2b orbit correction vector in radial, along-track, and cross-track components. BDS-3 PPP-B2b satellite orbits refer to the antenna phase center (APC) of B3I, while GPS PPP-B2b satellite orbits refer to the antenna phase center of L1/L2 ionosphere-free combination. It is worth noting that the IODC of the broadcast ephemeris changes as the ephemeris is updated and there is a time delay in the update of IODN. The users should keep applying the historical broadcast ephemeris until the IODN from the latest correction is updated under the circumstances.

The PPP-B2b real-time satellite clock offset can be obtained using Eq. (3):

$$t_{sat} = t_{brdc} - \frac{C_0}{c}, \tag{3}$$

where t_{sat} is the PPP-B2b real-time precise satellite clock offset. t_{brdc} is the satellite clock offset generated from the broadcast ephemeris. C_0 is the PPP-B2b clock correction. c is the velocity of light. To ensure the accuracy, the clock offset corrections must be matched with both broadcast ephemeris and satellite orbit corrections. Due to the different update frequencies of orbit and clock corrections, there may be a temporary mismatch when the IOD of orbit and clock corrections (IOD Corr) parameters are changed. In this case, the previous valid clock correction matched with the orbit correction should continue to be used.

Table 1 lists the types of DCB for BDS-3 satellites broadcasted by B2b signal. Since the PPP-B2b clock

Table 1 Types of DCB broadcasted by B2b signal

System	Number	Type of DCB
BDS-3	7	B1I–B3I, B1C(D)–B3I, B1C(P)–B3I, B2a(D)–B3I, B2a(P)–B3I, B2b(I)–B3I, B2b(Q)–B3I

offsets refer to B3I signal, the corrected clock offsets include the satellite pseudo-range hardware delay of B3I. When using multi-frequency observations, this bias needs to be eliminated as follows:

$$\hat{P}^s_{r,i} = P^s_{r,i} - DCB_i, \tag{4}$$

where $\hat{P}^s_{r,i}$ is the corrected pseudo-range observation of the certain frequency i between receiver r and satellite s. $P^s_{r,i}$ is the observed pseudo-range value between receiver r and satellite s. DCB_i is the DCB corrections of the frequency i in meters.

Multi-frequency real-time PPP model with PPP-B2b corrections

The raw pseudo-range and carrier phase observations can form the basic GNSS observation equations, and further construct different PPP models (Leick et al. 2015). When using PPP-B2b real-time satellite orbits and clock corrections, the basic observation equations for BDS-3 satellites at frequency k can be expressed as follows:

$$\begin{cases} P^s_{r,k} = \rho^s_r + c(t_r - \hat{t}^s_{B2b}) + m^s_{r,w} Z_{r,w} + \gamma_k I^s_{r,1} + b_{r,k} - (b^s_k - b^s_{B3I}) + e^s_{r,k} \\ \lambda_k \varphi^s_{r,k} = \rho^s_r + c(t_r - \hat{t}^s_{B2b}) + m^s_{r,w} Z_{r,w} - \gamma_k I^s_{r,1} + \lambda_k (N^s_{r,k} + B_{r,k} - B^s_k) + b^s_{B3I} + \varepsilon^s_{r,k} \end{cases}, \tag{5}$$

where $P^s_{r,k}$ and $\varphi^s_{r,k}$ are the observations of pseudo-range and carrier phase between receiver r and satellite s at frequency k. ρ^s_r is the geometric distance between satellite s and receiver r. t_r is the receiver clock offset. $\hat{t}^s_{B2b}$ is the satellite clock offset corrected by PPP-B2b corrections. $m^s_{r,w}$ is the corresponding mapping function and $Z_{r,w}$ is the zenith wet tropospheric delay. γ_k is the ionospheric mapping factor, $\gamma_k = \lambda_k^2 / \lambda_1^2$. $\hat{I}^s_{r,1}$ stands for the ionospheric delay of the first frequency, which is B3I for BDS-3 satellites. λ_k and $N^s_{r,k}$ stand for the wavelength and the integer ambiguity of frequency k. $B_{r,k}$ and B^s_k are the carrier phase hardware delays at frequency k of the receiver and satellite. $b_{r,k}$ and b^s_k are the pseudo-range hardware delays at frequency k of the receiver and satellite in meters. $e^s_{r,k}$ and $\varepsilon^s_{r,k}$ are the observation noise, multipath errors and other unmodeled errors of the pseudo-range and carrier phase, respectively. The other effects, including phase windup (Wu et al. 1992), relativistic effect (Ashby 2003), troposphere hydrostatic delay (Saastamoinen 1972) and solid earth tide (Petit and Luzum 2010) can be corrected with the existing models, so they are not mentioned in Eq. (5). It's worth noting that the satellite and receiver antenna phase center offsets (PCOs) are corrected by the IGS ANTEX file called igs20.atx (IGS 2022). The satellite phase center variations (PCVs) are not applied due to the lack of BDS-3 PCVs in igs20.atx.

Instead of using the ionosphere-free (IF) combination, we employ an undifferenced multi-frequency PPP model by estimating the ionosphere delay as a parameter. Due to the PPP-B2b clock offset product, an additional satellite pseudo-range hardware delay of B3I is involved in the model. To ensure the accuracy of the model, we need to handle the hardware delay of various frequencies appropriately (Håkansson et al. 2017). When the user chooses the dual-frequency solution, $b^s_k - b^s_{B3I}$ can be corrected by the PPP-B2b DCB according to Eq. (4). $b_{r,k}$ can be completely absorbed by the receiver clock offset and ionospheric delay. To represent this in mathematical terms, we reorganize the parameters and express the user-side dual-frequency model as:

$$\begin{aligned} P^s_{r,k} &= \rho^s_r + c(\hat{t}_r - \hat{t}^s_{B2b}) + m^s_{r,w} Z_{r,w} + \gamma_k \hat{I}^s_{r,1} + e^s_{r,k} \lambda_k \varphi^s_{r,k} \\ &= \rho^s_r + c(\hat{t}_r - \hat{t}^s_{B2b}) \\ &\quad + m^s_{r,w} Z_{r,w} - \gamma_k \hat{I}^s_{r,1} + \lambda_k \hat{N}^s_{r,k} + \varepsilon^s_{r,k} \end{aligned} \tag{6}$$

with

$$\begin{cases} \hat{t}_r = t_r + (\alpha_{12} b_{r,1} + \beta_{12} b_{r,2})/c \\ \hat{I}^s_{r,1} = I^s_{r,1} + \beta_{12}\left(b_{r,1} - b_{r,2}\right) \\ \hat{N}^s_{r,k} = N^s_{r,k} + \left(B_{r,k} - B^s_k\right) + \left[-\left(\alpha_{12} b_{r,1} + \beta_{12} b_{r,2}\right) + \gamma_k \beta_{12}\left(b_{r,1} - b_{r,2}\right)\right] / \lambda_k \\ \alpha_{ij} = \dfrac{f_i^2}{f_i^2 - f_j^2}, \beta_{ij} = -\dfrac{f_j^2}{f_i^2 - f_j^2} \end{cases}. \tag{7}$$

When GNSS observations at the third frequency or more are added, the effect caused by the pseudo-range hardware delay is different from the first two frequencies and can't be completely absorbed by the receiver clock offset and ionospheric delay. This error will have a significant impact on positioning accuracy. To eliminate such inconsistency, we require an additional inter-frequency bias parameter (IFB) (Deng et al. 2020; Zhou et al. 2023). The rest of the receiver pseudo-range hardware delay at multi-frequency can be eventually absorbed by IFB. To

simplify the form of the parameters, we also use PPP-B2b DCB to correct the satellite pseudo-range hardware delay at all frequencies. The multi-frequency observation equation based on PPP-B2b corrections can be expressed as:

$$\begin{aligned} P^s_{r,k} &= \rho^s_r + c\cdot\hat{t}_r + IFB_{k>2} - c\cdot\hat{t}^s_{B2b} + m^s_{r,w}Z_{r,w} \\ &\quad + \gamma_k\hat{I}^s_{r,1} + e^s_{r,k}\lambda_k\varphi^s_{r,k} = \rho^s_r + c(\hat{t}_r - \hat{t}^s_{B2b}) \\ &\quad + m^s_{r,w}Z_{r,w} - \gamma_k\hat{I}^s_{r,1} + \lambda_k\hat{N}^s_{r,k} + \varepsilon^s_{r,k} \end{aligned} \tag{8}$$

with

$$IFB_{k>2} = \left(b_{r,k} - b_{r,1}\right) + \frac{\beta_{12}}{\beta_{1k}}\left(b_{r,1} - b_{r,2}\right), \tag{9}$$

where $IFB_{k>2}$ is the IFB parameter at frequency k in meters, which is estimated using random walk with the model:

$$IFB_{k>2,t} = IFB_{k>2,t-1} + \varpi_{t-1},\ \varpi_{t-1} \sim N(0, q^2_{IFB}\Delta t), \tag{10}$$

where t and $t-1$ represent the current and previous epochs, respectively. q_{IFB} is the power spectral density of the noise of $IFB_{k>2}$. Considering the stability of DCB, q_{IFB} is set to 0.001 m with a 30 s sampling interval for the third, fourth and fifth signals. If n satellites are observed per epoch at k ($k>2$) frequencies, all parameters to be estimated in one epoch are as follows:

$$X = \left[\, X_{3\times1}\ \ \hat{t}_r\ \ IFB_{k-2}\ \ I_n\ \ ZWD\ \ N_{k\times n}\,\right]. \tag{11}$$

In this study, we have applied an extended Kalman filter to solve all the parameters according to Eq. (11) in real-time.

Data collections and processing strategies

In this study, the Sino M300 Pro receiver, which can track GPS/GLONASS/BDS/Galileo satellites, was used to collect PPP-B2b corrections for a total of 14 days from DOY 63 to DOY 78 (missing data at DOY 71 and DOY 77) in 2023. In addition, multi-frequency GNSS observation data from 7 IGS stations are used to assess the PPP performance. The observations were collected from DOY 63 to DOY 78 in 2023, with a sampling interval of 30 s. Figure 1 shows the distribution of the selected stations. The red line in the figure indicates the PPP-B2b service area. The selected IGS stations can track all five BDS-3 signals. The receiver and antenna information of these stations is listed in Table 2.

The processing strategies for multi-frequency PPP are described in Table 3. The precise satellite orbit, clock offset and DCB are generated from received PPP-B2b messages. It's worth noting that some stations provide C1X and C5X observations. Since the DCBs of these two observations are not provided in the PPP-B2b products, we use C1P and C5P DCB instead. The reference coordinates of selected stations are obtained from IGS weekly solutions. All observation data are processed in dual-frequency, triple-frequency, quad-frequency and five-frequency mode, respectively. The signal combinations for each mode are mentioned in Table 3. For the convenience of the following description, we use the F2, F3, F4 and F5 to represent the dual-frequency, triple-frequency, quad-frequency and five-frequency processing based on PPP-B2b corrections, respectively. For the analysis, the convergence time is defined as the time it takes to reach below 0.3 m and 0.6 m horizontal and vertical accuracy for at least 5 min, respectively.

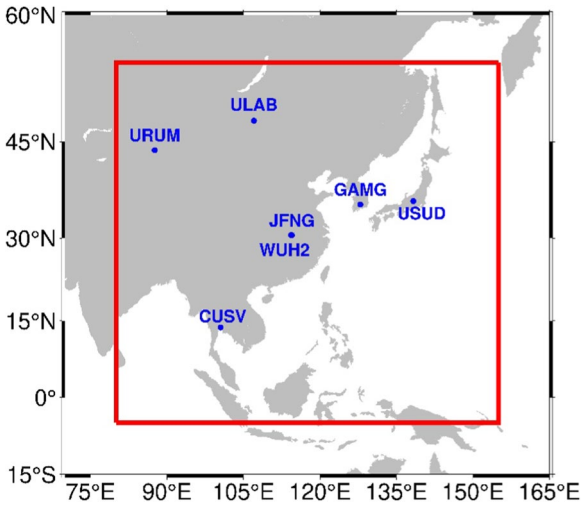

Fig. 1 The selected experimental stations from IGS network

Table 2 Receiver and antenna information of the selected stations

Stations	Receiver type	Antenna type
CUSV	JAVAD TRE_3	JAVRINGANT_DM
JFNG	TRIMBLE ALLOY	TRM59800.00
GAMG	SEPT POLARX5TR	LEIAR25.R4
ULAB	JAVAD TRE_3	JAVRINGANT_G5T
URUM	JAVAD TRE_3	JAVRINGANT_G5T
USUD	SEPT POLARX5	AOAD/M_T
WUH2	JAVAD TRE_3	JAVRINGANT_G5T

Result

BDS-3 PPP-B2b corrections assessment

The final precise products released by IGS Wuhan University Analysis Center (abbreviated as WHU) are used as the reference to assess the quality of PPP-B2b real-time satellite orbits and clock offsets. Also, the products from IGS RTS are employed for further

Table 3 Data processing strategy

Item	Correction model or estimation strategy
Satellite orbit	CNAV1 broadcast ephemeris + PPP-B2b orbit corrections
Satellite clock offset	CNAV1 broadcast ephemeris + PPP-B2b clock offset corrections
Satellite DCB	PPP-B2b DCB corrections
Cutoff elevation	10°
Weighing strategies	Elevation-dependent weighing model; 3 mm and 0.3 m for raw phase and pseudo-range, respectively (Ge et al. 2008)
Ionosphere	Estimated as random walk ($9m^2/s$)
Troposphere	Zenit dry delay is corrected by Saastamoinen model (Saastamoinen 1972), zenith wet delay is estimated as random walk ($2.5 \times 10^{-7} m^2/s$) and Global Mapping Function is used (Böhm et al. 2006)
Receiver clock offset	Estimated as white noise
Phase windup	Corrected (Ashby 2003)
inter-frequency bias	Estimated as random walk ($1 \times 10^{-6} m^2/s$)
Receiver positions	Static mode: estimated as constants; Kinematic mode: estimated as white noise process
Experimental schemes	F2: B1I/B3I F3: B1I/B3I/B2a F4: B1I/B3I/B2a/B1C F5: B1I/B3I/B2a/B1C/B2b
Ambiguity	Estimated as a float constant

comparison. It should be noted that the precise orbits from WHU are referred to the center-of-mass (CoM) of the satellite, while the PPP-B2b orbits are referred to the satellite antenna phase center. Therefore, the PCOs between the WHU orbits and the PPP-B2b orbits need to be corrected using igs20.atx.

The BDS-3 satellites orbit errors of PPP-B2b service and broadcast ephemeris on March 11, 2023 are presented in Fig. 2. The top, medium and bottom panels of Fig. 2 show the satellite orbit errors in radial, along-track, and cross-track components, respectively. Different colors represent different satellites.

As shown in Fig. 2, the accuracy of PPP-B2b real-time orbits is improved compared with that of the broadcast ephemeris, and the errors in all three directions are slightly reduced. Meanwhile, the satellite orbits calculated before and after the broadcast ephemeris update have obvious jumps. The PPP-B2b corrections can reduce this jump. Therefore, the time series of PPP-B2b orbit error is more continuous compared with the orbit errors generated from the broadcast ephemeris.

The accuracy of the orbits from broadcast ephemeris, PPP-B2b real-time orbits and IGS RTS orbits of BDS-3 are shown in Fig. 3. The average RMSs of orbit errors are listed in Table 4. From the results, the RMS of PPP-B2b

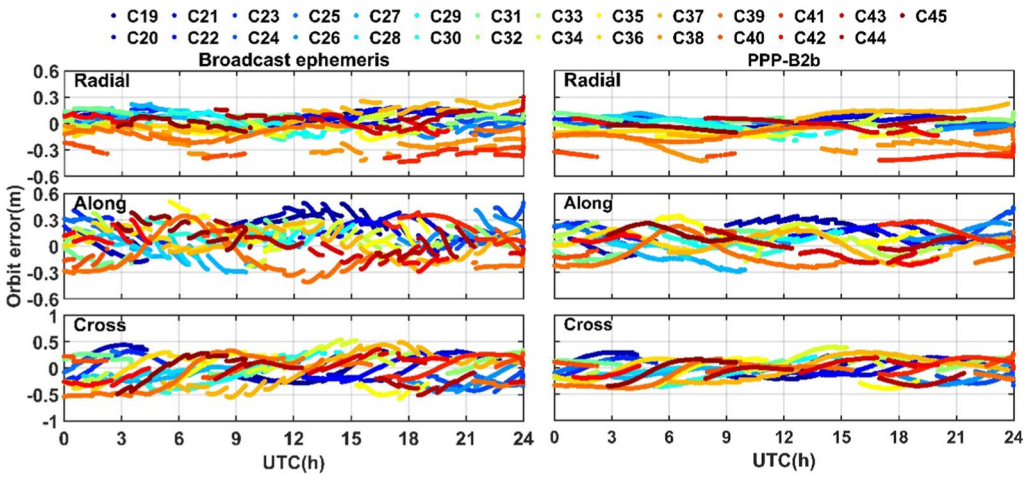

Fig. 2 Time series of BDS-3 satellite orbit error generated from broadcast ephemeris (left) and PPP-B2b corrections (right)

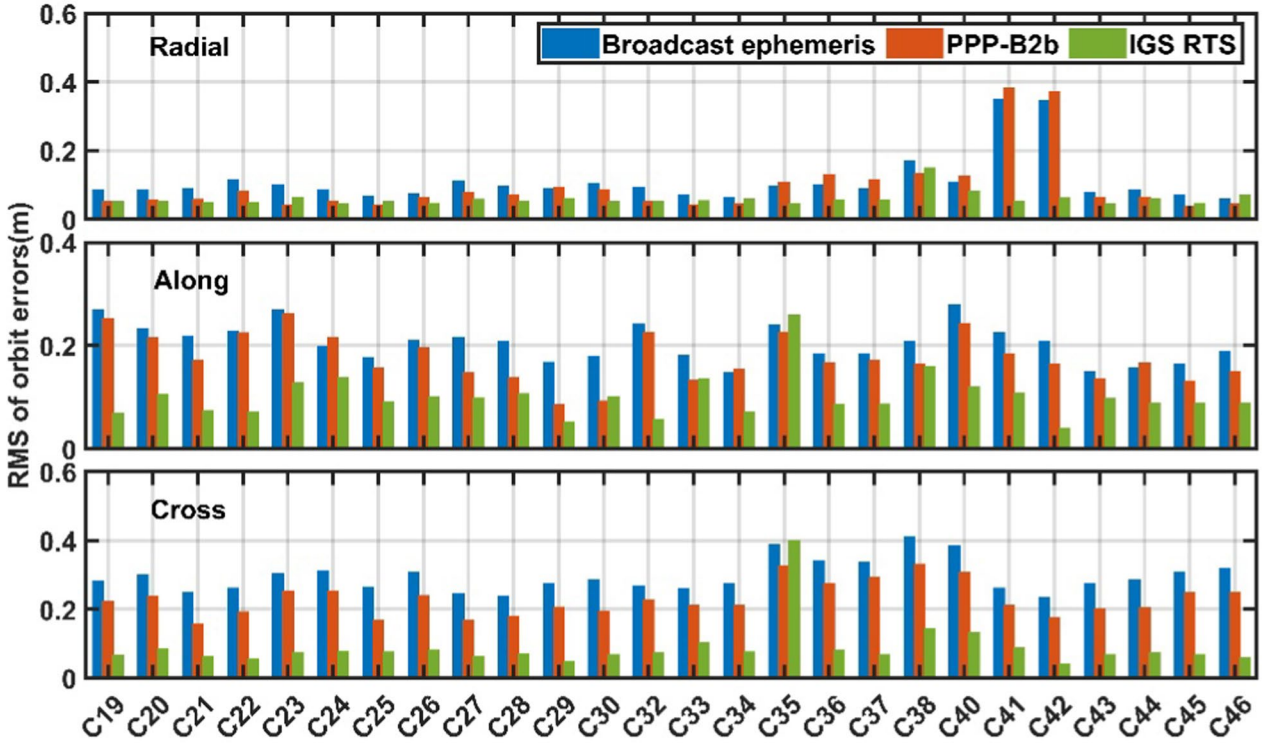

Fig. 3 RMS of BDS-3 satellites orbit generated from broadcast ephemeris, PPP-B2b corrections, and IGS real-time products

Table 4 RMS of BDS-3 satellite orbit accuracy for different products (unit: cm)

Product type	Radial	Along-track	Cross-track	3D
Broadcast	10.7	20.2	29.1	37.1
PPP-B2b	9.2	17.3	22.5	29.8
IGS RTS	5.5	9.8	8.5	14.1

orbit errors are 9.2 cm, 17.3 cm, 22.5 cm in radial, along-track, and cross-track components, respectively, which are reduced by 14.0%, 14.4%, and 22.7% compared with the broadcast ephemeris. The accuracy of RTS orbits is better than PPP-B2b real-time orbits. The PPP-B2b orbit errors of C41 and C42 are 0.3 ~ 0.4 m in radial component, which are significantly higher than other satellites. This may relate to the PCO corrections released by IGS.

In terms of clock evaluation, the final precise clock offsets from WHU are used as reference. The BDS-3 satellite clock offset from WHU refers to B1I/B3I IF combination, while the PPP-B2b real-time clock offset refers to B3I signal. Therefore, the PPP-B2b DCB should be applied to eliminate the inconsistency before the comparison. Moreover, the clock datum differences between the clock offset products from different analysis centers will cause systematical biases during evaluation (Montenbruck et al. 2015). In order to eliminate these biases, the same reference satellite is chosen to calculate the single-difference clock offsets for comparison (Yao et al. 2017). In multi-frequency positioning, the systematical biases can be absorbed by the ambiguity parameter and do not affect the positioning results. The stability of the satellite clock, however, will significantly affect positioning accuracy and convergence time (Zhou et al. 2022; Jinhuo et al. 2022). Figure 4 shows the STD values of BDS-3 satellite clock offset errors. From Fig. 4, it can be seen that the STD of PPP-B2b real-time clock offsets is about 0.1–0.2 ns, which is significantly better than that of broadcast ephemeris and IGS RTS products.

To evaluate the accuracy of PPP-B2b DCB values, we use the precise DCB products released by the Chinese Academy of Sciences (CAS) as reference (Wang et al. 2016). Figure 5 shows the average differences of PPP-B2b DCB values including B3I-B1I, B3I-B1C (P) and B3I-B2a (P), respectively.

As shown in Fig. 5, the DCB values of each code are consistent with CAS products. The largest bias is around 2 ns. The mean values of the B3I-B1I, B3I-B1C (P), and B3I-B2a (P) DCB differences are 0.65 ns, 0.46 ns, and 0.64 ns, respectively.

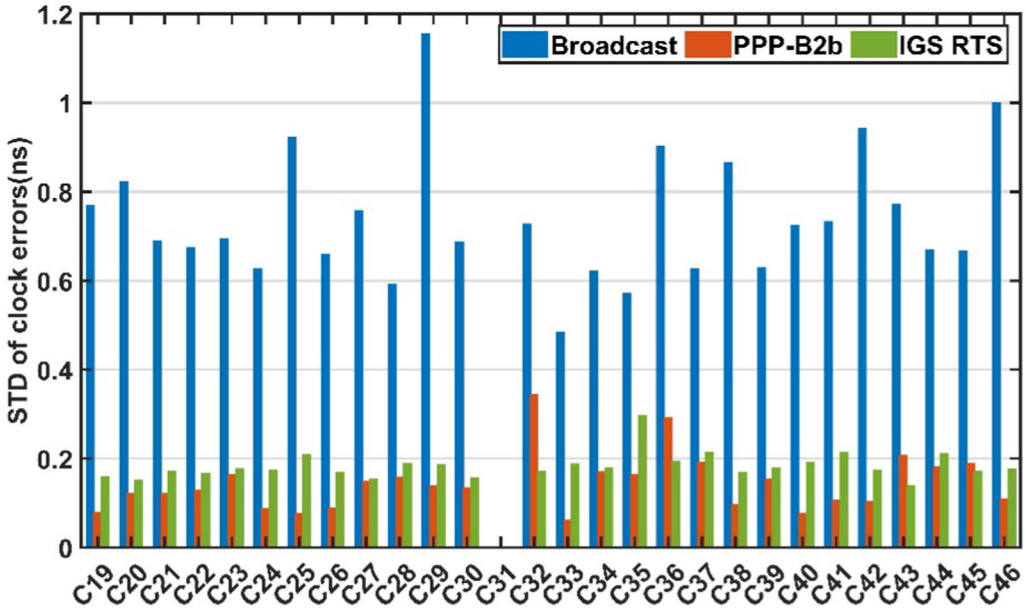

Fig. 4 STD of clock offset difference for broadcast ephemeris, PPP-B2b products and RTS IGS

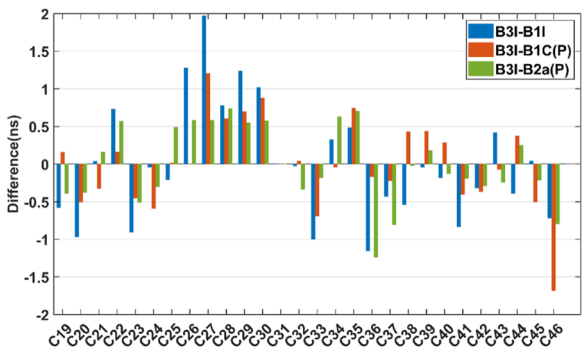

Fig. 5 Mean difference between PPP-B2b DCB and CAS products

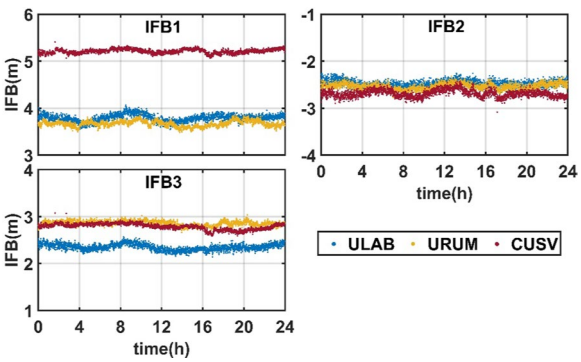

Fig. 6 Time series of estimated IFBs of three stations for multi-frequency model (DOY 67, 2023)

Dual-frequency to five-frequency BDS-3 PPP results

In this part, the performance of the static and kinematic five-frequency PPP using PPP-B2b corrections is evaluated. We use IFB1, IFB2 and IFB3 to represent the IFB parameter corresponding to the third, fourth and fifth frequency, respectively. The time series of estimated IFBs at ULAB, URUM, CUSV station on DOY 67, 2023 are shown in Fig. 6. The figure shows that IFBs of different frequencies remain stable within a day. It's appropriate to model IFB parameter as the random walk in the multi-frequency model using PPP-B2b service. According to Eq. (9), the IFB parameter is a combination of the receiver hardware delay. Therefore, the IFB estimates are different because of the different receiver types. It's worth noting that due to the same receiver and antenna type, the IFB values of ULAB and URUM are close. Figure 7 shows the differences between estimated IFBs and reference IFBs generated from receiver DCB products released by CAS. The STD and RMS of IFBs are listed in Table 5. The estimated IFBs and the reference IFBs have good consistency. The statistics results illustrate that the STD values of IFBs are around 6–8 cm while the RMS values are around 10–30 cm. The estimated IFBs are able to partially absorb other errors that are not fully modeled and residual error of PPP-B2b product. This reason can explain the relatively higher RMS values.

Figure 8 presents the total number of visible BDS-3 satellites (red line) and available satellites (green line)

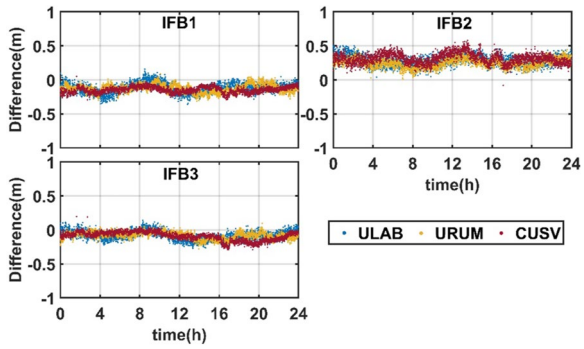

Fig. 7 Differences between estimated IFBs and reference IFBs generated from receiver DCB products of three stations (DOY 67, 2023)

Table 5 STD and RMS of IFBs (DOY 67, 2023)

Item	STD (m)	RMS (m)
IFB1	0.061	0.145
IFB2	0.072	0.290
IFB3	0.061	0.104

for PPP-B2b positioning at two stations on DOY 67 in 2023, respectively. As shown in Fig. 8, the average number of visible satellites per day remains stable in general, with about 11 ~ 15 BDS-3 satellites. Due to the distribution of regional tracking networks, PPP-B2b service can't support all the BDS-3 satellites at the same time. The number of available satellites with valid orbit and clock corrections that can be used for PPP-B2b positioning is about 6–11. It should be noted that the number of available satellites at 8:00 and 16:00 is below 6, which seriously affects the positioning performance.

The static positioning errors of GAMG and ULAB station using PPP-B2b service in the east (E), north (N), and up (U) components from DOY 63 to DOY 78, 2023 are presented in Fig. 9. The PPP-B2b messages are missing in DOY 71 and DOY 77 so the PPP are not available for these two days. The positioning results of each model can obtain the positioning accuracy of 0.3 m in the horizontal direction and 0.6 m in the vertical direction within 20 min. All solutions can achieve centimeter-level positioning results after convergence, with errors of about 2–4 cm in the E and N components and 4–7 cm in the U component.

The RMS errors and convergence time of 14-day static positioning results for the F2, F3, F4 and F5 models using PPP-B2b service are shown in Figs. 10 and 11, respectively. The line in the middle of the boxplot represents the median of dataset. The average RMS errors and convergence time for different models are summarized in Table 6. From the statistical results, it is observed that the median convergence time for each model is less than 15 min and the convergence time of all solutions does not exceed 20 min. The F5 model can achieve the best positioning accuracy in E, N and U components valued 4.6, 1.9 and 5.1 cm, respectively. The 3D error reduced from 7.7 to 7.1 cm compared with the F2 model. The positioning accuracy of the F4 and F5 models has a slight improvement in the U component compared with the other models, and the improvement in E and N components is not obvious. The average convergence time of the F5 model is 7.2 min, which is reduced by 25.8% compared with the F2 model. Although more observations are used in the F4 and F5 models, the positioning performance is not significantly improved after convergence.

The kinematic positioning errors of GAMG and ULAB station for the F2, F3, F4 and F5 models using PPP-B2b service from DOY 63 to DOY 78, 2023 are presented in Fig. 12. The results show that the kinematic PPP result is at the decimeter level using the PPP-B2b corrections.

Figures 13 and 14 displays the boxplot of the RMS errors in three components and convergence time for F2, F3, F4 and F5 models, respectively. The average RMS errors and convergence time of PPP-B2b solutions are summarized in Table 7. From the results, the F3–F5 models have better convergence performance and

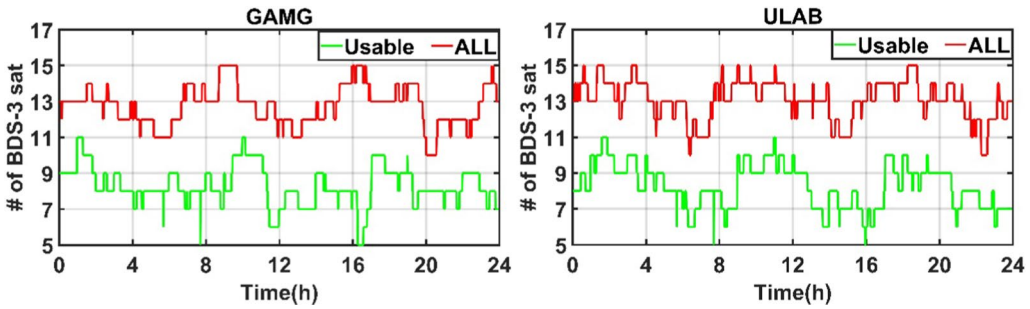

Fig. 8 Number of all visible satellites and available satellites for PPP-B2b positioning at GAMG (left panel) and ULAB (right panel) station on DOY 067 in 2023

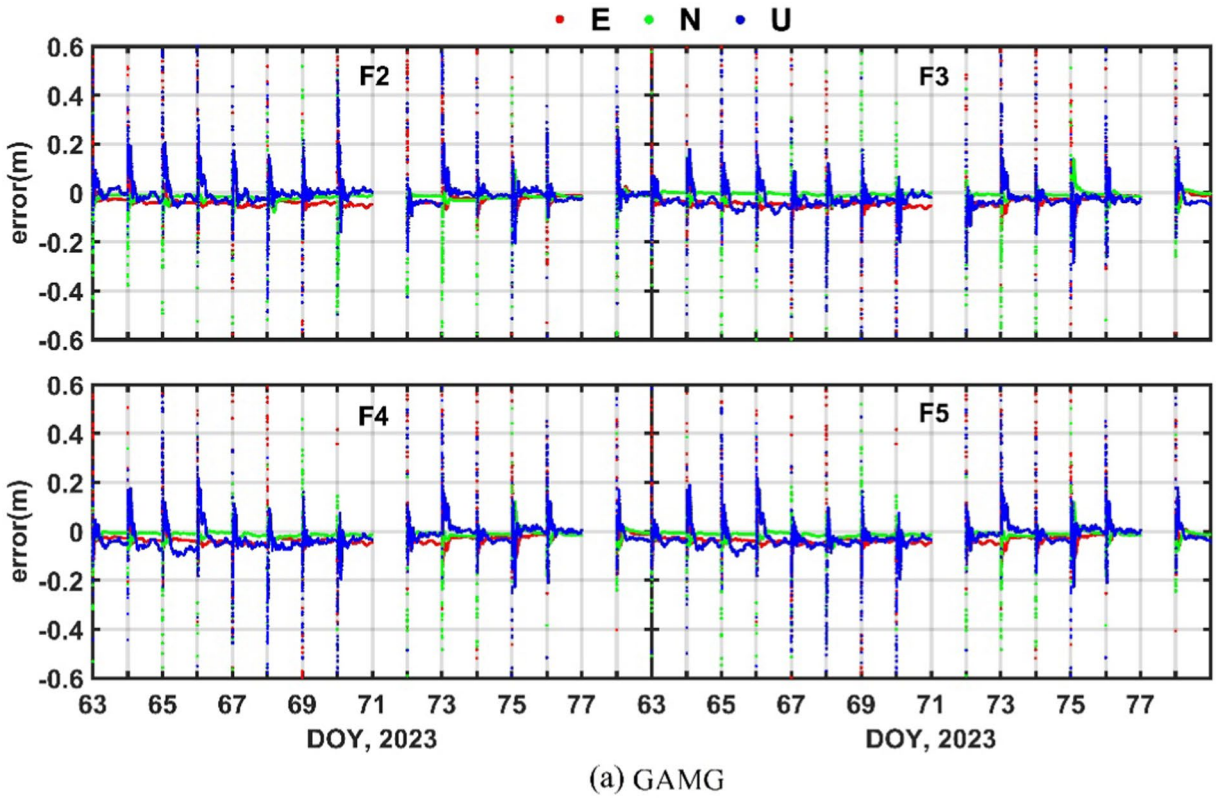

(a) GAMG

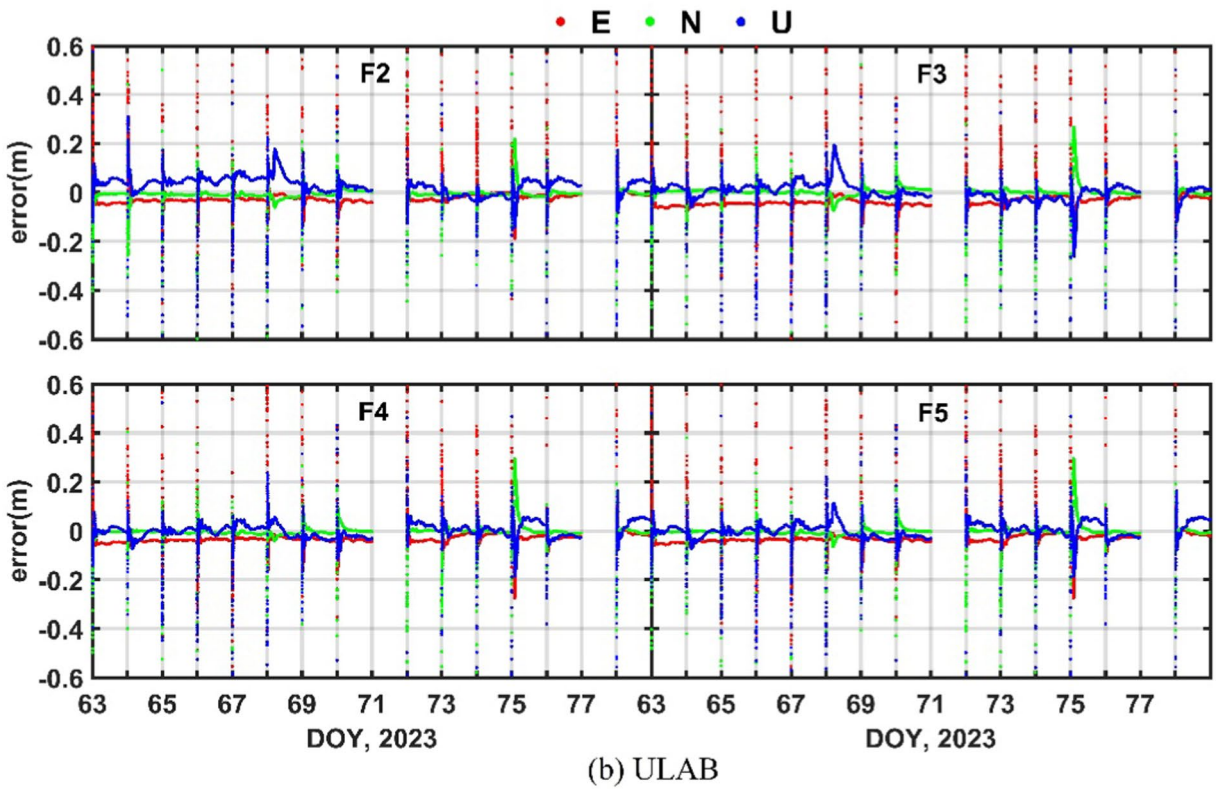

(b) ULAB

Fig. 9 Static PPP results using PPP-B2b service from DOY 63 to DOY 78 in 2023

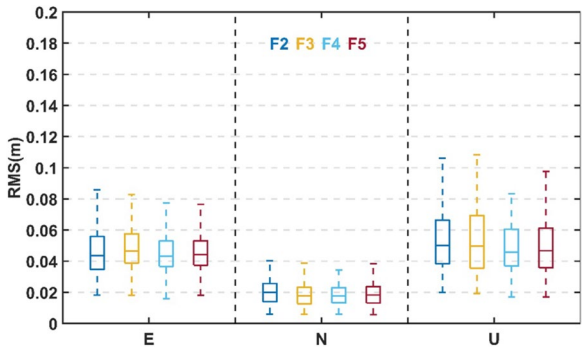

Fig. 10 Boxplot of the accuracy of static PPP for selected stations

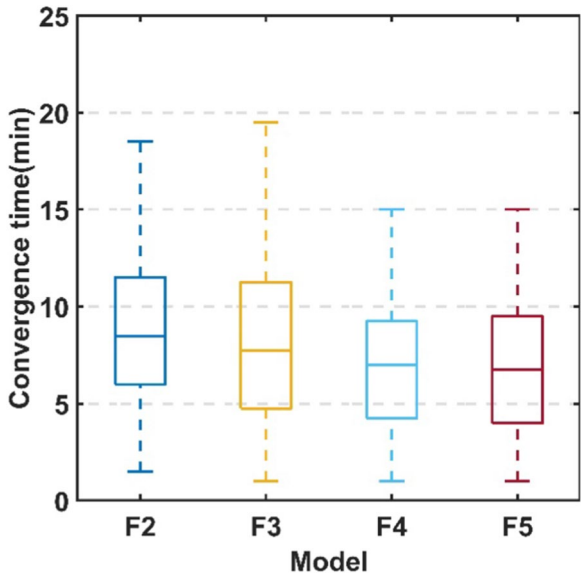

Fig. 11 Boxplot of the convergence time of static PPP for selected stations

Table 6 The average RMS errors and convergence time of static PPP

Model	E (cm)	N (cm)	U (cm)	3D (cm)	Convergence time (min)
F2	4.66	2.16	5.74	7.70	9.7
F3	4.75	1.91	5.58	7.57	8.9
F4	4.61	1.97	5.15	7.19	7.2
F5	4.56	1.92	5.12	7.12	7.2

positioning accuracy than the F2 model. The average convergence time of the F3 model is 20.5 min, which is 15.6% faster than that of the F2 model. However, the F5 model has only an 9.2% reduction in convergence time compared to the F3 model and is almost the same as the F4 model.

In order to further explore the contribution of multi-frequency model, Fig. 15 shows the convergence performance of kinematic PPP with PPP-B2b corrections under a 68.2% confidence level. From Fig. 15, we can find that during the first 30 min, the F4 and F5 model have the best convergence performance. It takes 12.5 min for the F4 and F5 model to reduce the error in the horizontal and vertical directions to 0.4 m and 0.6 m, respectively, while that for the F3 and F2 model are 16.5 min and 23.5 min. The F2 model takes about twice as long as the F5 model. After 60 min, the PPP results of all models have fully converged to the centimeter-level values. There are little differences between the results of F2 ~ F5 models thereafter. We find that the F4 and F5 model are able to play a greater role at the beginning of PPP-B2b processing, and this contribution gradually decreases after convergence.

In terms of positioning accuracy, the RMS errors of the F5 model in the E, N, and U components are 7.1 cm, 4.8 cm, and 12.4 cm, respectively. Table 7 indicates that the RMS errors of the F5 model are reduced by 6.8%, 11.5%, and 5.5%, respectively, compared with the F2 model. The performances of the F4 model are comparable to that of the F5 model after convergence, and both are better than the F2 model. The statistical results indicate that multi-frequency model can improve not only convergence time but also three-dimensional positioning accuracy of PPP-B2b service.

Conclusions

The BDS-3 PPP-B2b service has promoted the implementation of real-time PPP in environments where the Internet is unavailable or unstable. In this contribution, we employed a multi-frequency PPP model using BDS-3 PPP-B2b service and first analyzed the dual-frequency to five-frequency PPP performance based on PPP-B2b corrections in both static and kinematic modes.

Compared with the broadcast satellite orbit, the PPP-B2b real-time orbit is more continuous, with average RMS error of 9.2 cm, 17.3 cm, 22.5 cm in radial, along-track, and cross-track components, respectively. PPP-B2b orbit corrections can reduce the satellite orbit error and discontinuity caused by ephemeris updates. The STD of the BDS-3 PPP-B2b clock offset is about 0.1–0.2 ns, which is better than both broadcast ephemeris and IGS RTS products. The PPP-B2b DCB products show good consistency with final DCB products from CAS. The average values of DCB differences of each signal are about 0.4 ~ 0.6 ns.

Positioning experiments with dual-frequency, triple-frequency, quad-frequency and five-frequency observations are conducted using PPP-B2b corrections, respectively. The time series of estimated IFBs are stable over time and show good consistency with

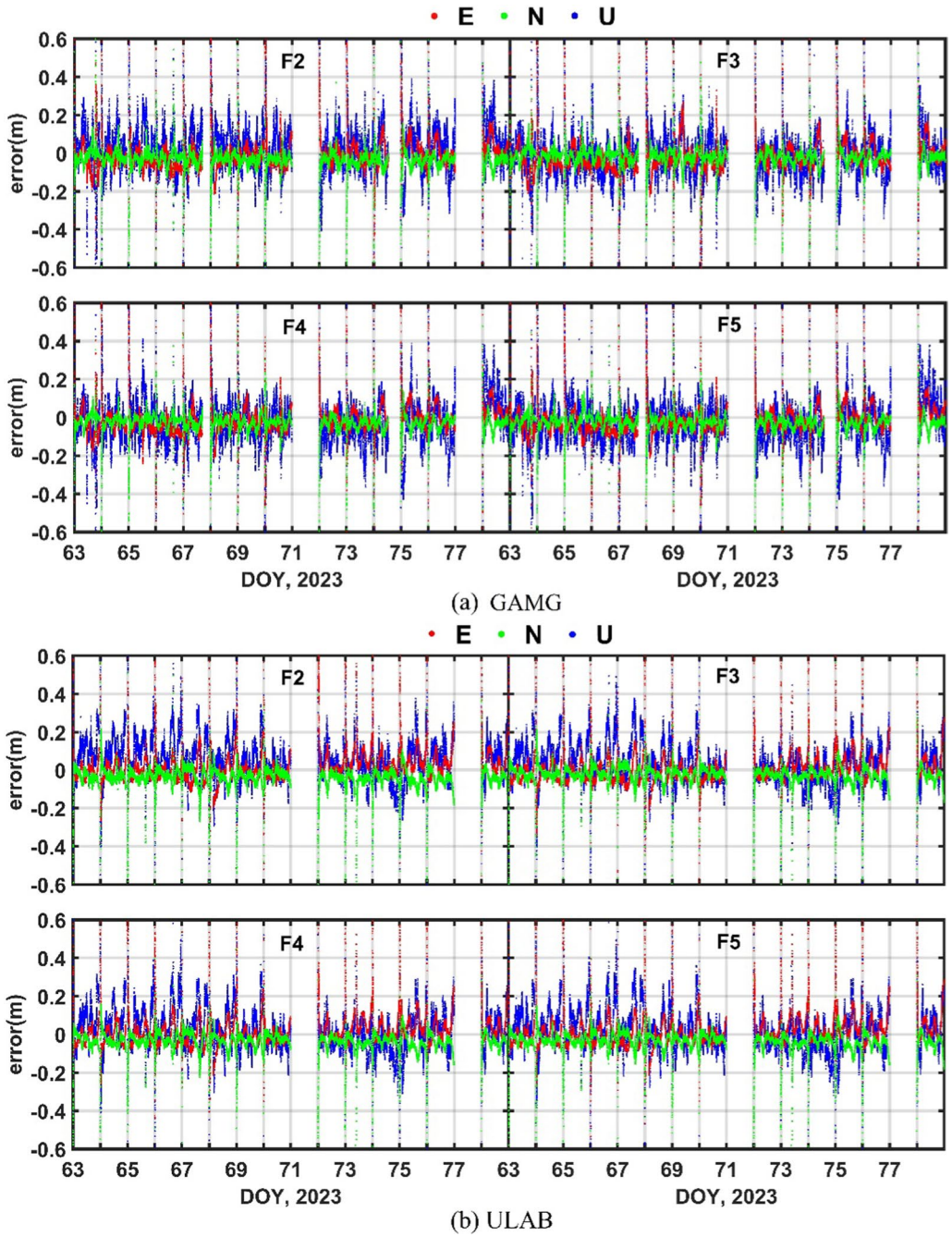

Fig. 12 Kinematic PPP results using PPP-B2b service from DOY 63 to DOY 78 in 2023

the reference IFBs. The static solutions of dual-frequency to five-frequency PPP models can reach the centimeter-level accuracy after convergence, with errors of 2–4 cm in the E and N components and 4–7 cm in the U component. The median convergence time of each model does not exceed 15 min. The F5 model has the best positioning performance. In terms of kinematic mode, the average convergence time of the F3–F5 models is about 18–20 min, which is significantly reduced by around 22% compared to the F2 model. The 3D positioning RMS of the F2, F3, F4, and F5 models are 16.15 cm, 15.00 cm, 15.18 cm, and 15.11 cm, respectively. At the convergence stage of the PPP-B2b solution, the F4 and F5 model have better convergence performance than the F3 and F2 model with smaller positioning errors. The achieved experimental

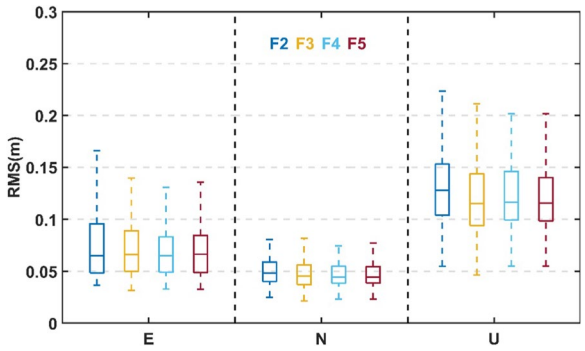

Fig. 13 Boxplot of the accuracy of kinematic PPP for selected stations

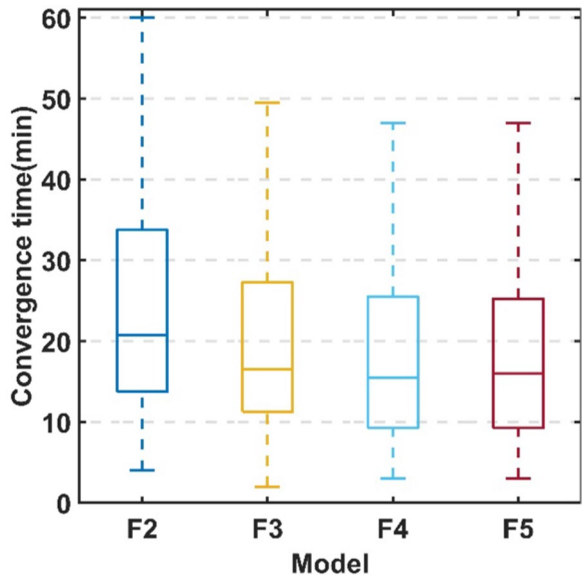

Fig. 14 Boxplot of the convergence time of kinematic PPP for selected stations

Table 7 The average RMS errors and convergence time of kinematic PPP

Model	E (cm)	N (cm)	U (cm)	3D (cm)	Convergence time (min)
F2	7.66	5.40	13.16	16.15	24.3
F3	7.39	4.88	12.11	15.00	20.5
F4	7.06	4.79	12.56	15.18	18.7
F5	7.14	4.78	12.43	15.11	18.6

results indicate that multi-frequency observations can improve both convergence time and three-dimensional positioning accuracy in PPP-B2b solutions. In addition, the contribution of multi-frequency observations is greater in the convergence stage compared to that after

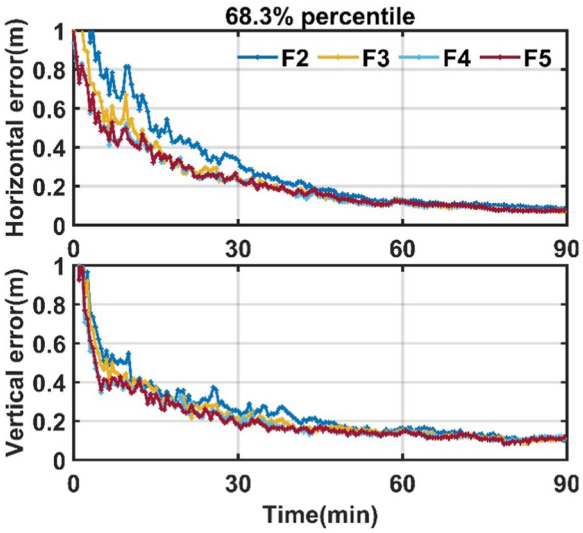

Fig. 15 Convergence performance of kinematic PPP with PPP-B2b corrections under 68.2% confidence level

convergence. In the future, the combination of more public satellite-based PPP services, such as Galileo HAS and QZSS CLAS, will meet the real-time demands of more GNSS users for higher precision.

Acknowledgements
The numerical calculations have been done on the supercomputing system in the Supercomputing Center of Wuhan University. The IGS WHU Analysis Center, CAS are also appreciated for providing access to GNSS products and GNSS observations.

Author contributions
YH performed the data analysis and drafted the manuscript. RX and ZX discussed the data and critically revised the manuscript. LM proof-read the submission. All authors read and approved the final manuscript.

Funding
This research was funded by the National Natural Science Foundation of China (no. 42174031, no.42230104), the Fundamental Research Funds for the Central Universities, the Special Fund of Hubei Luojia Laboratory under Grant 2201000038, and the Knowledge Innovation Program of Wuhan-Shuguang.

Availability of data and materials
GNSS observation data from International GNSS Service can be accessed from https://cddis.nasa.gov/archive/gnss/data/daily/ (registration required). The final precise products released by IGS Wuhan University Analysis Center are available on ftp://igs.gnsswhu.cn/pub/gnss/products. Relevant DCB products are available on https://cddis.nasa.gov/archive/gnss/products/mgex/dcb. The igs20.atx is obtained from https://files.igs.org/pub/station/general/pcv_archive/.

Declarations

Competing interests
The authors declare that they have no competing interests.

Author details
[1]School of Geodesy and Geomatics, Wuhan University, Wuhan 430079, Hubei, China. [2]Hubei Luojia Laboratory, Wuhan University, Wuhan 430079, Hubei, China. [3]Chinese Antarctic Center of Surveying and Mapping, Wuhan University, Wuhan 430079, Hubei, China.

Received: 1 March 2024 Accepted: 21 May 2024
Published online: 11 June 2024

References

Ashby N (2003) Relativity in the global positioning system. Living Rev Relat 6:1–42. https://doi.org/10.12942/lrr-2003-1

Böhm J, Niell A, Tregoning P et al. (2006) Global Mapping Function (GMF): a new empirical mapping function based on numerical weather model data. Geophys Res Lett 33. https://doi.org/10.1029/2005GL025546

Booth JS, Snow RN (2009) An evaluation of OmniStar XP and PPP as a replacement for DGPS in airborne applications. In: Proceedings of the 22nd International Technical Meeting of the Satellite Division of The Institute of Navigation (ION GNSS 2009). pp. 1188–1194

Chen J, Zhang Y, Yu C et al (2022) Models and performance of SBAS and PPP of BDS. Satell Navigat 3:4. https://doi.org/10.1186/s43020-022-00065-3

CSNO (2020a) Navigation Satellite System Signal In Space Interface Control Document Precise Point Positioning Service Signal PPP-B2b (Version 1.0)

CSNO (2020b) Specifications for open service performance of BeiDou navigation satellite system, Beijing

Dai L, Chen Y, Lie A et al. (2016) StarFire™ SF3: worldwide centimeter-accurate real time GNSS positioning. In: Proceedings of the 29th International Technical Meeting of the Satellite Division of The Institute of Navigation (ION GNSS+ 2016). pp. 3295–3320. https://doi.org/10.33012/2016.14673

Deng C, Liu Q, Zou X et al (2020) Investigation of tightly combined single-frequency and single-epoch precise positioning using multi-GNSS data. Remote Sens 12:285. https://doi.org/10.3390/rs12020285

Elsobeiey M, Al-Harbi S (2016) Performance of real-time precise point positioning using IGS real-time service. GPS Solut 20:565–571. https://doi.org/10.1007/s10291-015-0467-z

Fernandez-Hernandez I, Chamorro-Moreno A, Cancela-Diaz S et al (2022) Galileo high accuracy service: initial definition and performance. GPS Solut 26:1–18. https://doi.org/10.1007/s10291-022-01247-x

Ge M, Gendt G, Rothacher MA et al (2008) Resolution of GPS carrier-phase ambiguities in precise point positioning (PPP) with daily observations. J Geodesy 82:389–399. https://doi.org/10.1007/s00190-007-0187-4

Geng T, Li Z, Xie X et al (2022) Real-time ocean precise point positioning with BDS-3 service signal PPP-B2b. Measurement 203:111911. https://doi.org/10.1016/j.measurement.2022.111911

Håkansson M, Jensen AB, Horemuz M et al (2017) Review of code and phase biases in multi-GNSS positioning. GPS Solut 21:849–860. https://doi.org/10.1007/s10291-016-0572-7

Hao M, Jiao W, Jia X et al. (2020) Precise point positioning performance evaluation of QZSS centimeter level augmentation service. In: China Satellite Navigation Conference (CSNC) 2020 Proceedings 9. https://doi.org/10.1007/978-981-15-3715-8_8

He Q, Chen L, Liu L et al (2023) Long-term performance evaluation of BeiDou PPP-B2b products and its application in time service. Remote Sens 15:1358. https://doi.org/10.3390/rs15051358

Huang L, Meng X (2021) Accuracy analysis of precise point positioning using BDS-3 PPP-B2b signals. J Geodesy Geodynam 41:516–519. https://doi.org/10.14075/j.jgg.2021.05.014

IGS (2022) [IGSMAIL-8238] Upcoming switch to IGS20/igs20.atx and repro3 standards. https://lists.igs.org/pipermail/igsmail/2022/008234.html

Ilaria M, Melania S, Luca C et al. (2023) Galileo high accuracy service performance and anomaly mitigation capabilities. GPS Solut 28. https://doi.org/10.1007/s10291-023-01555-w

Jin S, Su K (2020) PPP models and performances from single-to quad-frequency BDS observations. Satell Navigat 1:1–13. https://doi.org/10.1186/s43020-020-00014-y

Jinhuo L, Chengpan T, Shanshi Z et al. (2022) The bias in PPP-B2b real-time clock offset and the strategy to reduce it. Remote Sens 14. https://doi.org/10.3390/rs14184569

Kazmierski K, Zajdel R, Sośnica K (2020) Evolution of orbit and clock quality for real-time multi-GNSS solutions. GPS Solut J Global Navigat Satell Syst 24:111. https://doi.org/10.1007/s10291-020-01026-6

Kouba J, Héroux P (2001) Precise point positioning using IGS orbit and clock products. GPS Solut 5:12–28. https://doi.org/10.1007/PL00012883

Leandro R, Landau H, Nitschke M et al. (2011) RTX positioning: the next generation of cm-accurate real-time GNSS positioning. In: Proceedings of the 24th international technical meeting of the satellite division of the Institute of Navigation (ION GNSS 2011). pp. 1460–1475

Leick A, Rapoport L, Tatarnikov D (2015) GPS satellite surveying. Wiley, USA

Li X, Li X, Liu G et al (2020) BDS multi-frequency PPP ambiguity resolution with new B2a/B2b/B2a+ b signals and legacy B1I/B3I signals. J Geodesy 94:1–15. https://doi.org/10.1007/s00190-020-01439-8

Liu Y, Yang C, Zhang M (2022) Comprehensive analyses of PPP-B2b performance in China and surrounding areas. Remote Sens 14. https://doi.org/10.3390/rs14030643

Montenbruck O, Steigenberger P, Hauschild A (2015) Broadcast versus precise ephemerides: a multi-GNSS perspective. GPS Solut 19:321–333. https://doi.org/10.1007/s10291-014-0390-8

Naciri N, Yi D, Bisnath S et al (2023) Assessment of Galileo high accuracy service (HAS) test signals and preliminary positioning performance. GPS Solut 27:73. https://doi.org/10.1007/s10291-023-01410-y

Namie H, Okamoto O, Kubo N et al (2018) Initial performance evaluation of centimeter-class augmentation system using Quasi-Zenith Satellite System. Electron Commun Japan 101:3–10

Petit G, Luzum B (2010) IERS technical note No. 36, IERS conventions (2010). International Earth Rotation and Reference Systems Service. Frankfurt, Germany

Ren Z, Gong H, Peng J et al (2021) Performance assessment of real-time precise point positioning using BDS PPP-B2b service signal. Adv Space Res 68:3242–3254. https://doi.org/10.1016/j.asr.2021.06.006

Rovira-Garcia A, Timoté CC, Juan JM et al. (2021) Ionospheric corrections tailored to the Galileo High Accuracy Service. J Geodesy 95. https://doi.org/10.1007/s00190-021-01581-x

Saastamoinen J (1972) Atmospheric correction for the troposphere and stratosphere in radio ranging satellites. Use Artif Satell Geodesy 15:247–251. https://doi.org/10.1029/GM015p0247

Song W, Zhao X, Lou Y et al. (2021) Performance evaluation of BDS-3 PPP-B2b Service. In: Geomatics and Information Science of Wuhan University. 1–11. https://doi.org/10.13203/j.whugis20200686

Sun S, Wang M, Liu C et al (2023) Long-term performance analysis of BDS-3 precise point positioning (PPP-B2b) service. GPS Solut 27:69. https://doi.org/10.1007/s10291-023-01409-5

Tang C, Hu X, Chen J et al. (2022) Orbit determination, clock estimation and performance evaluation of BDS-3 PPP-B2b service. J Geodesy 96. https://doi.org/10.1007/s00190-022-01642-9

Tao J, Liu J, Hu Z et al. (2021) Initial assessment of the BDS-3 PPP-B2b RTS compared with the CNES RTS. GPS Solut 25. https://doi.org/10.1007/s10291-021-01168-1

Wang N, Yuan Y, Li Z et al (2016) Determination of differential code biases with multi-GNSS observations. J Geodesy 90:209–228. https://doi.org/10.1007/s00190-015-0867-4

Wu J-T, Wu SC, Hajj GA et al (1992) Effects of antenna orientation on GPS carrier phase. Astrodynamics 1991:1647–1660

Wu Z, Wang Q, Hu C et al (2022) Modeling and assessment of five-frequency BDS precise point positioning. Satell Navigat 3:8. https://doi.org/10.1186/s43020-022-00069-z

Wu P, Lou Y, Zhang W et al (2023) Evaluation of real-time kinematic positioning performance of the BDS-3 PPP service on B2b signal. GPS Solut 27:1–14. https://doi.org/10.1007/s10291-023-01532-3

Xu X, Nie Z, Wang Z et al (2023) An improved BDS-3 PPP-B2b positioning approach by estimating signal in space range errors. GPS Solut 27:110. https://doi.org/10.1007/s10291-023-01455-z

Xu Y, Yang Y, Li J (2021) Performance evaluation of BDS-3 PPP-B2b precise point positioning service. GPS Solut 25. https://doi.org/10.1007/s10291-021-01175-2

Yang Y, Gao W, Guo S et al (2019) Introduction to BeiDou-3 navigation satellite system. Navigation 66:7–18. https://doi.org/10.1002/navi.291

Yang Y, Ding Q, Gao W et al (2022) Principle and performance of BDSBAS and PPP-B2b of BDS-3. Satell Navigat 3:1–9. https://doi.org/10.1186/s43020-022-00066-2

Yao Y, He Y, Yi W et al (2017) Method for evaluating real-time GNSS satellite clock offset products. GPS Solut 21:1417–1425. https://doi.org/10.1007/s10291-017-0619-4

Zhang X, Hu J, Ren X (2020) New progress of PPP/PPP-RTK and positioning performance comparison of BDS/GNSS PPP. Acta Geod Cartogr Sin. 49:1084–1100. https://doi.org/10.11947/j.AGCS.2020.20200328

Zhang Y, Kubo N, Pullen S (2022) Evaluation of QZSS centimeter level augmentation system (CLAS): open-sky to urban environments and geodetic to low-cost receivers. In: Proceedings of the 35th International Technical Meeting of the Satellite Division of The Institute of Navigation (ION GNSS+ 2022). pp. 2729–2750

Zhou H, Wang L, Fu W et al (2022) Real-time single-frequency precise point positioning using BDS-3 PPP-B2b corrections. Measurement 205:112178. https://doi.org/10.1016/j.measurement.2022.112178

Zhou H, Fu W, Wang L et al (2023) Multi-frequency BDS-3 real-time positioning performance assessment using new PPP-B2b augmentation service. IEEE Sens J. https://doi.org/10.1109/JSEN.2023.3235901

Zumberge J, Heflin M, Jefferson D et al (1997) Precise point positioning for the efficient and robust analysis of GPS data from large networks. J Geophys Res Solid Earth 102:5005–5017. https://doi.org/10.1029/96JB03860

Publisher's Note